

Electronic Supplementary Information

On Exo-Cyclic Aromaticity

Tamal Goswami, Manoswita Homray, Satadal Paul, Debojit Bhattacharya, Anirban Misra*

Department of Chemistry, University of North Bengal, Darjeeling 734013, India

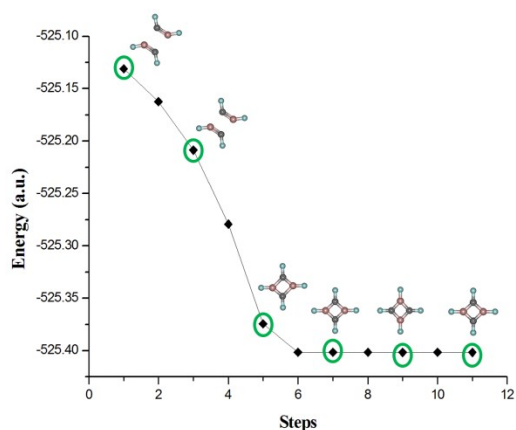
*Phone: +919434228745; Email: anirbanmisra@yahoo.com

Item	Description	Page
Table S1	The optimized bond lengths (in Å) at different DFT and <i>ab initio</i> methodologies using aug-cc-pVDZ basis set.	2
Fig. S1	Geometry convergence during optimization of C ₂ B ₂ F ₄ from (a) rectangular and (b) non-planar starting geometries and their corresponding final energies at B3LYP/aug-cc-pVDZ level. The points for which the geometries are presented in the plot are circled in green.	2
Fig. S2	Variation of total energy of C ₂ B ₂ F ₄ at T = 300 K along a DFT-based molecular dynamics simulation of 5 ps.	3
Fig. S3	Variation of kinetic energy of C ₂ B ₂ F ₄ at T = 300 K along a DFT-based molecular dynamics simulation of 5 ps.	4
Fig. S4	Variation of potential energy of C ₂ B ₂ F ₄ at T = 300 K along a DFT-based molecular dynamics simulation of 5 ps.	5
Table S2	The nucleus-independent chemical shift (NICS) values (ppm) in the ring plane [NICS (0)] and 1 Å above the ring plane [NICS (1)] at different DFT and <i>ab initio</i> methodologies using aug-cc-pVDZ basis set.	6
Fig. S5	The π - (a) and σ - (b) current density vector plots.	7
	Computational Details	8
	Calculation of Ring Strain Energy(RSE)	8
	Calculation of Aromatic Stabilization Energy	9
Table S3	The optimized geometries, minimum harmonic frequencies, NICS (0) and NICS (1) values of C ₂ B ₂ F ₂ H ₂ , C ₂ B ₂ Cl ₄ , C ₂ B ₂ Br ₄ and C ₂ B ₂ I ₄ at B3LYP/aug-ccpVDZ level.	10
Table S4	AdNDP orbitals along with occupations for the designed C ₂ B ₂ Cl ₄ and C ₂ B ₂ Br ₄ systems.	11

Table S1. The optimized bond lengths (in Å) at different DFT and *ab initio* methodologies using aug-cc-pVDZ basis set.

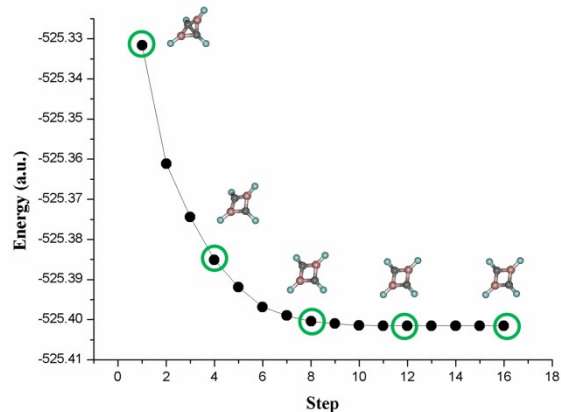
Methodology (along with aug-cc-pVDZ basis set)	B-C bond length (in Å)	B-F bond length (in Å)	C-F bond length (in Å)	∠BCB bond angle (in °)	∠CBC bond angle (in °)	∠CBBC dihedral angle (in °)	Energy (in A.U.)	Minimum vibrational frequency (in cm ⁻¹)
QCISD*	1.542	1.340	1.319	93.23	86.77	0.00	-524.09	58.58
CISD*	1.527	1.330	1.303	93.18	86.82	0.00	-524.07	52.36
CCSD*	1.541	1.338	1.317	93.22	86.78	0.00	-524.09	57.82
MP2	1.544	1.350	1.331	93.86	86.14	0.00	-524.18	56.54
B3LYP	1.532	1.339	1.322	93.42	86.58	0.00	-525.40	61.90
B3PW91	1.531	1.337	1.317	93.48	86.52	0.00	-525.19	58.27
PBEPBE	1.541	1.347	1.331	93.54	86.46	0.00	-524.86	60.36
BLYP	1.543	1.350	1.340	93.57	86.43	0.00	-525.33	65.22
TPSSH	1.534	1.342	1.326	93.52	86.47	0.00	-525.41	61.65
CAM-B3LYP	1.525	1.334	1.315	93.44	86.56	0.00	-525.23	57.91
M-06	1.526	1.329	1.310	93.42	86.58	0.00	-525.19	60.51

*Computed with cc-pVDZ basis set



(a)

Final Energy= -525.40156 a.u.



(b)

Final Energy= -525.40156 a.u.

Fig. S1 Geometry convergence during optimization of C₂B₂F₄ from (a) rectangular and (b) non-planar starting geometries and their corresponding final energies at B3LYP/aug-cc-pVDZ level. The points for which the geometries are presented in the plot are circled in green.

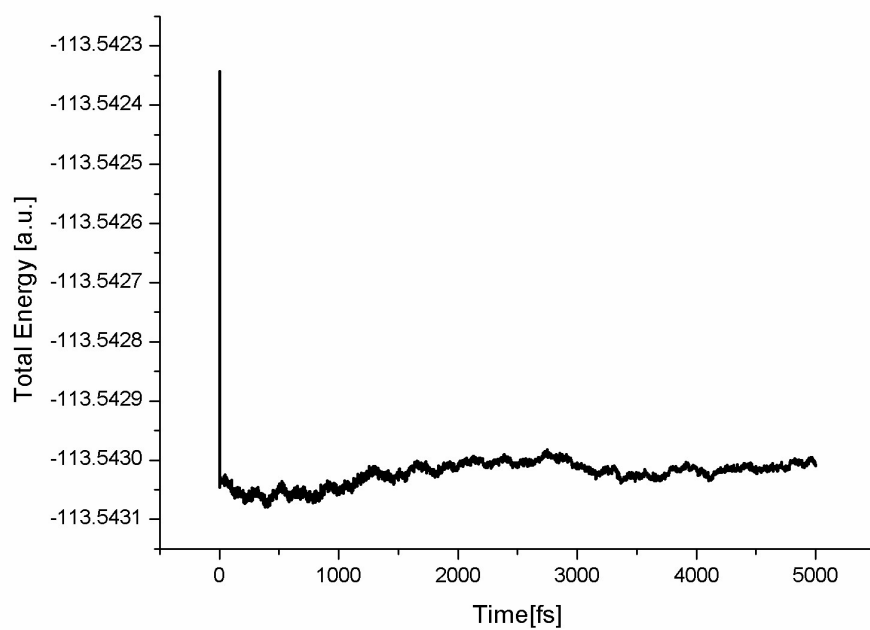


Fig. S2 Variation of total energy of $C_2B_2F_4$ at $T = 300$ K along a DFT-based molecular dynamics simulation of 5 ps.

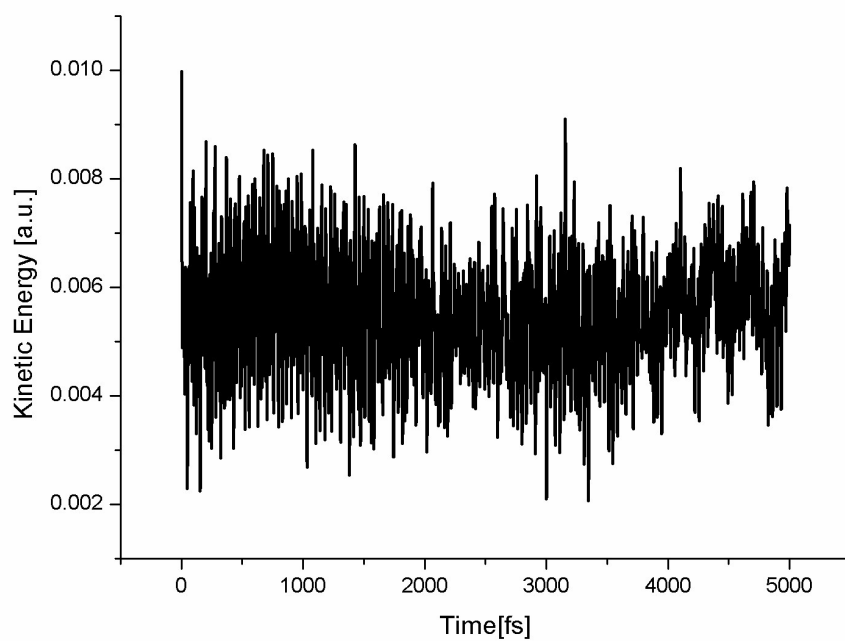


Fig. S3 Variation of kinetic energy of $C_2B_2F_4$ at $T = 300$ K along a DFT-based molecular dynamics simulation of 5 ps.

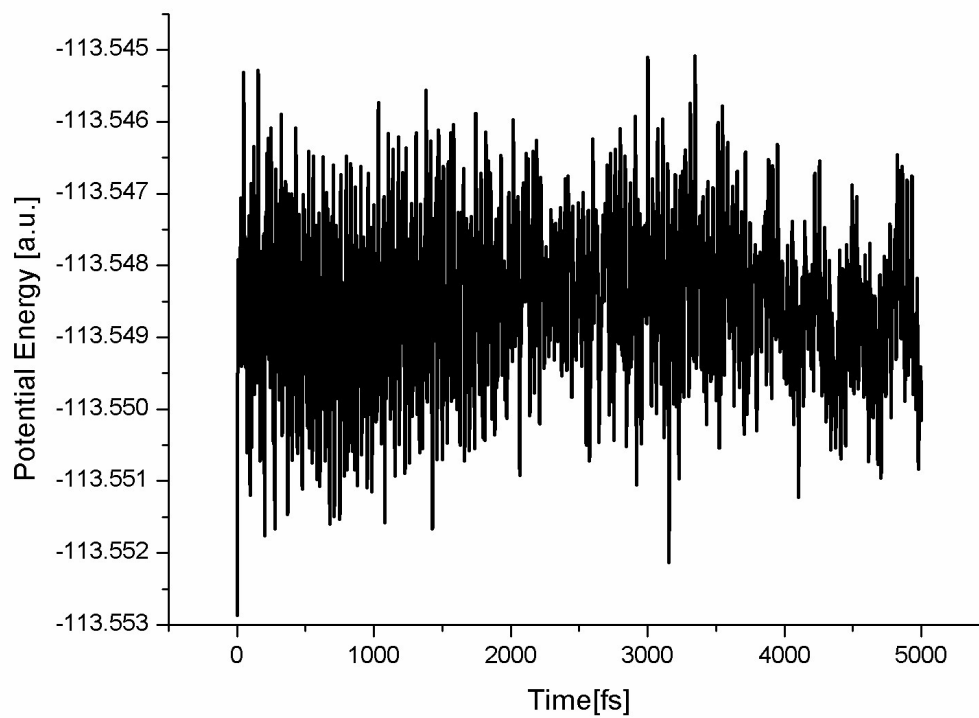
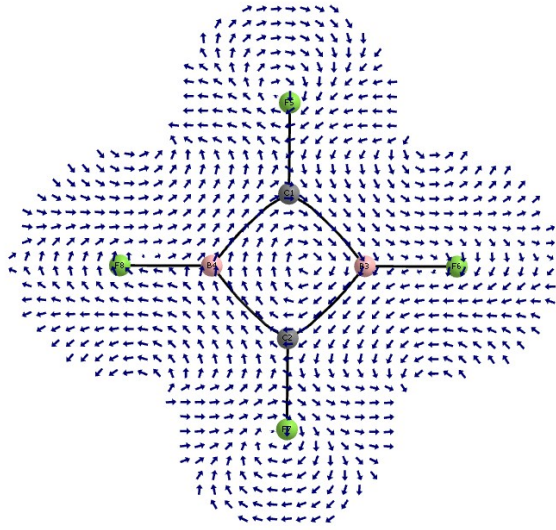


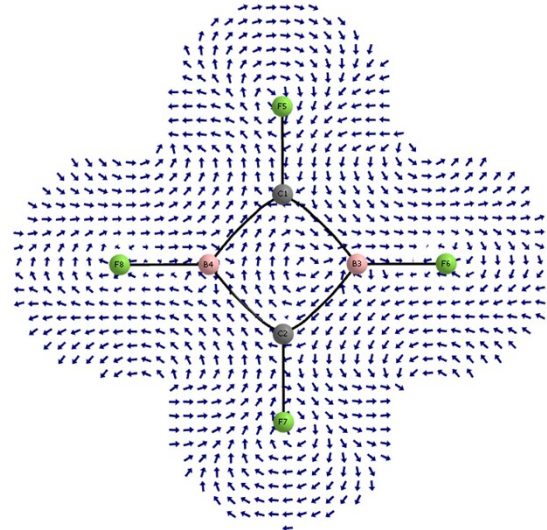
Fig. S4 Variation of potential energy of $C_2B_2F_4$ at $T = 300$ K along a DFT-based molecular dynamics simulation of 5 ps.

Table S2. The nucleus-independent chemical shift (NICS) values (ppm) in the ring plane [NICS (0)] and 1 Å above the ring plane [NICS (1)] at different DFT and *ab initio* methodologies using aug-cc-pVDZ basis set.

Methodology (along with aug-cc-pVDZ basis set)	NICS (0)	NICS (1)
B3LYP	-5.1673	-7.0986
B3PW91	-4.8444	-7.0370
PBEPBE	-3.3913	-6.2099
BLYP	-3.9376	-6.3329
CAM-B3LYP	-5.5683	-7.3992



(a)



(b)

Fig. S5 The π - (a) and σ - (b) current density vector plots.

Computational Details

The minimum energy search was performed in Gaussian 09W suit of software at different DFT and *ab initio* methodologies.^{S1} We have also used the ADF program^{S2} for energy decomposition analysis (EDA) based on the methods of Ziegler and Rauk.^{S3} The total binding energy ΔE released upon the formation of the molecule from atomic fragments is divided into two major components, namely, ΔE_{prep} and ΔE_{int} , i.e., $\Delta E = \Delta E_{prep} + \Delta E_{int}$. ΔE_{prep} corresponds to the energy needed to promote the separated fragments from their equilibrium geometry to the final structure in the molecule. The interaction energy ΔE_{int} between the fragments is further decomposed into three physically meaningful terms, $\Delta E_{int} = \Delta E_{elstat} + \Delta E_{pauli} + \Delta E_{orb}$. Here, ΔE_{elstat} is the classical electrostatic interaction between the promoted fragments as they are brought to their positions in the final complex. ΔE_{pauli} corresponds to the repulsive Pauli interaction between occupied orbitals on the two fragments in the molecule. ΔE_{orb} represents interactions between the occupied molecular orbitals of one fragment with the unoccupied molecular orbitals of the other fragment and also signifies the mixing of occupied and virtual orbitals within the same fragment.^{S3} Diradical character y_i was estimated by means of PUHF method with the formula $y_i = 1 - \frac{2T_i}{1+T_i^2}$. The diradical character is defined by the weight of the doubly excited configuration in multiconfigurational self consistent field (MCSCF) theory and formally expressed by the overlap (T_i) between localized natural orbitals [highest occupied MO (HOMO) – i and lowest unoccupied MO (LUMO) + i], i being the number of MOs.^{S4} The dissected canonical molecular orbital NICS (CMO-NICS)^{S5,S6} computation is performed using the ADF package. AdNDP is a compact combination of intuitive simplicity of Lewis theory with the flexibility and generality of Canonical Molecular Orbital theory thus providing a perfect description of systems featuring both localized and delocalized bonding without invoking the concept of resonance. AdNDP orbitals are analyzed using Multiwfn A Multifunctional Wave function Analysis.^{S7} Molecular dynamics simulations were carried out with CP2K/Quickstep^{S8} package, which consists Born-Oppenheimer MD (BOMD) BLYP^{S9,S10} GTH pseudopotentials^{S11,S12} with a combined Plane-Wave (280 Ry density cutoff) and TZV2P basis sets.

Calculation of Ring Strain Energy(RSE)

The ring strain energy can be calculated with the help of Bader's Quantum theory of Atoms in Molecules (QTAIM).^{S13} The kinetic energy density at the ring critical point (3,+1) can be utilized to estimate the ring strain energy.^{S14} For the calculation of the RSE a regression equation, $RSE = 337.72 \times G(r) - 8.115$, is used as described in Ref. S2. The calculated RSE is found to be 27.98 kcal/mol.

Calculation of Aromatic Stabilization Energy:

The aromaticity of the proposed molecule is deemed to contribute significantly to its inherent stability. Recently, the stabilization in the molecular energy due to electronic mobility has been equated with the aromatic stabilization energy in the frame of second order perturbation theory. The proposed theoretical framework makes use of the inter-site hopping integral (t_{ij}) and the onsite repulsion energy (U) to account for the electron delocalization. The electronic population engaged in delocalization is obtained as a product of spin – orbital population ($n_{i\sigma}$ and $n_{j\sigma'}$) within the unrestricted framework and the degree of delocalization, which is estimated from electron localization function (ELF).

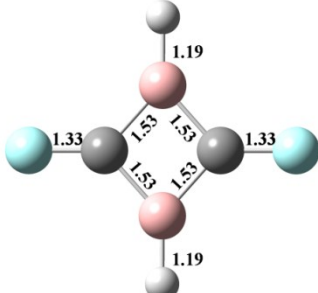
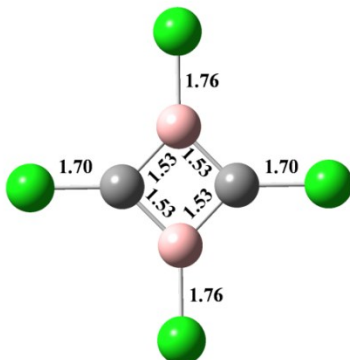
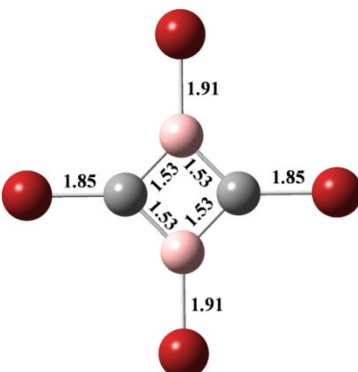
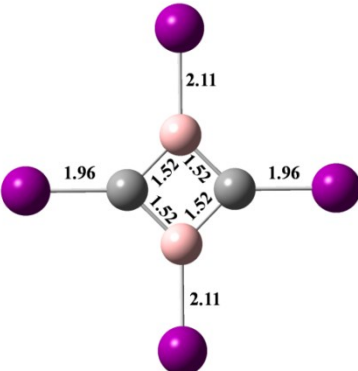
$$\Delta E = \sum_{i,j} \frac{t_{ij}^2}{U} (n_{i\sigma} n_{j\sigma'} + n_{i\sigma'} n_{j\sigma}) ELF^2$$

However, the above equation had been derived for standard aromatic molecules which differ significantly from the present system with respect to the electronic structure and type of aromaticity. Particularly, the itinerancy of the lone pair of electrons in between the boron and fluorine completes the loop of electronic circulation and thus makes the pattern of electron delocalization unique with respect to traditional aromatic systems. To comply with this picture of electron delocalization, the above equation is split into two parts as follows,

$$\Delta E = \sum_{C,B} \frac{t_{ij}^2}{U} (n_{C\sigma} n_{B\sigma'} + n_{C\sigma'} n_{B\sigma}) ELF^2 + \sum_{F,B} \frac{2t_{ij}^2}{U} (n_{F\sigma} n_{B\sigma'} + n_{F\sigma'} n_{B\sigma}) ELF^2$$

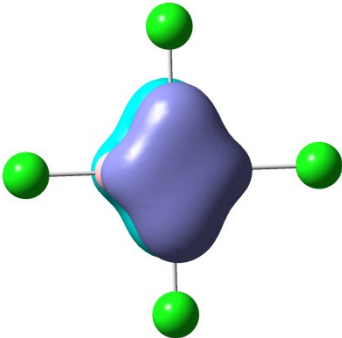
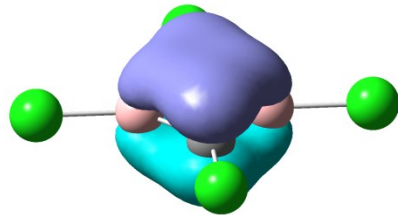
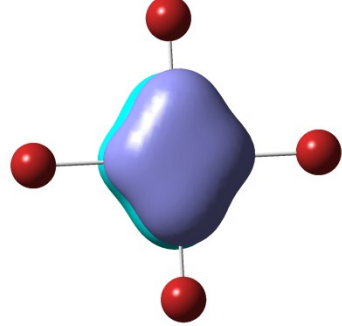
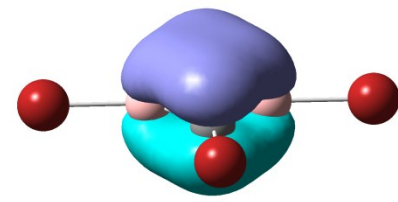
Here, the first part accounts for the electron delocalization within C – B ring, and the second part quantifies stabilization for electron delocalization within Lewis acid-base pair. The probability of both spin transfer from F to B is included by multiplying the stabilization term by two.

Table S3. The optimized geometries, minimum harmonic frequencies, NICS (0) and NICS (1) values of $C_2B_2F_2H_2$, $C_2B_2Cl_4$, $C_2B_2Br_4$ and $C_2B_2I_4$ at B3LYP/aug-ccpVDZ level*.

Species	Minimum Frequency	NICS (0)	NICS (1)
	29.93	3.1873	-7.4007
	23.52	7.3817	-6.1710
	7.97	10.1049	-5.9335
	20.30	18.2129	-5.0623

*As the aug-cc-pVDZ basis set is not available for the element I, Sapporo-DKH3-DZP-2012 is applied as an extrabasis on I atoms.

Table S4. AdNDP orbitals along with occupations for the designed $C_2B_2Cl_4$ and $C_2B_2Br_4$ systems.

System	Occupation Number	AdNDP Orbital	
		Front View	Side View
$C_2B_2Cl_4$	1.99		
$C_2B_2Br_4$	2.00		

In silico tests are performed with $C_2B_2Cl_4$, $C_2B_2Br_4$ and $C_2B_2I_4$ systems to examine the effect of $B \leftarrow X$ back donation on the aromaticity of $C_2B_2X_4$ with $X = F, Cl, Br$ and I . Harmonic frequency and NICS calculations are performed to assess their stability and aromaticity. The results are presented in Table S3. Low values of minimum vibrational frequencies make one sceptic about their viability at the first instance. Additionally the σ -antiaromaticity induces further instability of all these systems as is evident from the positive values of NICS (0). The $C_2B_2X_4$ systems show a decreasing trend in the NICS (1) value from fluorine to iodine (Table S2 and S3).

It is also to be noted that if $B \leftarrow X$ back donation is ignored, all the systems including $C_2B_2F_4$ at least possess 2 π -electrons which is capable to maintain the aromaticity in such systems. The AdNDP analyses clearly illustrate that there is no participation of back donated electrons to the aromatic electron cloud (Table S4). This observation substantiates the absence of back donation of π -electrons from higher p_z -orbitals of Cl ($3p_z$), Br ($4p_z$) and I ($5p_z$) to the empty $2p_z$ -orbital of the boron atom due to energy mismatch. Instead, inspection of the AdNDP orbitals can establish the involvement of only 2 π -electrons to the aromatic cloud unlike $C_2B_2F_4$. The AdNDP analysis for $C_2B_2I_4$ could not be performed due to lack of similar basis set for iodine compared to other atoms.

- S1. Gaussian 09, Revision B.01, M. J. Frisch, G. W. Trucks, H. B. Schlegel, G. E. Scuseria, M. A. Robb, J. R. Cheeseman, G. Scalmani, V. Barone, G. A. Petersson, H. Nakatsuji, X. Li, M. Caricato, A. Marenich, J. Bloino, B. G. Janesko, R. Gomperts, B. Mennucci, H. P. Hratchian, J. V. Ortiz, A. F. Izmaylov, J. L. Sonnenberg, D. Williams-Young, F. Ding, F. Lipparini, F. Egidi, J. Goings, B. Peng, A. Petrone, T. Henderson, D. Ranasinghe, V. G. Zakrzewski, J. Gao, N. Rega, G. Zheng, W. Liang, M. Hada, M. Ehara, K. Toyota, R. Fukuda, J. Hasegawa, M. Ishida, T. Nakajima, Y. Honda, O. Kitao, H. Nakai, T. Vreven, K. Throssell, J. A. Montgomery, Jr., J. E. Peralta, F. Ogliaro, M. Bearpark, J. J. Heyd, E. Brothers, K. N. Kudin, V. N. Staroverov, T. Keith, R. Kobayashi, J. Normand, K. Raghavachari, A. Rendell, J. C. Burant, S. S. Iyengar, J. Tomasi, M. Cossi, J. M. Millam, M. Klene, C. Adamo, R. Cammi, J. W. Ochterski, R. L. Martin, K. Morokuma, O. Farkas, J. B. Foresman, and D. J. Fox, Gaussian, Inc., Wallingford CT, 2009.
- S2. Amsterdam Density Functional (Theoretical Chemistry, Vrije Universiteit, Amsterdam, The Netherlands, <http://www.scm.com>).
- S3. T. Ziegler and A. Rauk, *Theor. Chim. Acta.*, 1977, **46**, 1-10.
- S4. K. Yamaguchi, *Self-Consistent Field: Theory and Applications*, Elsevier, Amsterdam, 1990.
- S5. C. Corminboeuf, T. Heine and J. Weber, *Phys. Chem. Chem. Phys.*, 2003, **5**, 246-251.
- S6. C. Corminboeuf, R. B. King and P. v. R. Schleyer, *Chem. Phys. Chem.*, 2007, **8**, 391-398.
- S7. T. Lu and F. Chen, *J. Comp. Chem.*, 2012, **33**, 580-592.
- S8. J. VandeVondelea, M. Krackb, F. Mohamedb, M. Parrinellob, T. Chassaingc and J. Hutter, *Comput. Phys. Commun.*, 2005, **167**, 103-128.
- S9. A. D. Becke, *Phys. Rev. A*, 1988, **38**, 3098-3100.
- S10. C. Lee, W. Yang and R. G. Parr, *Phys. Rev. B*, 1988, **37**, 785-789.
- S11. S. Goedecker, M. Teter and J. Hutter, *Phys. Rev. B*, 1996, **54**, 1703-1710.
- S12. C. Hartwigsen, S. Goedecker and J. Hutter, *Phys. Rev. B*, 1998, **58**, 3641-3662.
- S13. R.F.W. Bader, *Atoms in Molecules: A Quantum Theory*, Oxford University Press, Oxford, UK, 1990.
- S14. A. Bauzá, D. Quiñonero, P. M. Deyà, A. Frontera, *Chem. Phys. Lett.*, 2012, **536**, 165-169.

